ELSEVIER

Journal of Quantitative Spectroscopy & Radiative Transfer 107 (2007) 331–339

Journal of Quantitative Spectroscopy & Radiative Transfer

www.elsevier.com/locate/jqsrt

Note

Absorption spectroscopy of formaldehyde at 1.573 μm

Weixiong Zhao, Xiaoming Gao*, Lunhua Deng, Teng Huang, Tao Wu, Weijun Zhang

Anhui Institute of Optics and Fine Mechanics, The Chinese Academy of Sciences, Hefei 230031, PR China

Received 13 December 2006; received in revised form 24 January 2007; accepted 26 January 2007

Abstract

The absorption spectrum of formaldehyde at 1.573 μm has been recorded at room temperature with a typical sensitivity of 6×10^{-8} cm^{-1} by using an off-axis integrated cavity output spectroscopy set-up based on a distributed feedback diode laser. More than 140 lines have been recorded within the laser spectral range (6351.3−6362.1 cm^{-1}). The corresponding spectral parameters (i.e. line positions and line intensities) are presented.

Keywords: Formaldehyde; Near-infrared spectrum; Off-axis integrated absorption spectroscopy; Line parameters

1. Introduction

Formaldehyde (H_2CO) is a key atmospheric constituent that is photochemically active in the troposphere, making it a source of HO_x (OH and HO_2), and thus plays a significant role in the interrelated chemistries of ozone and the HO_x and NO_x (NO and NO_2) cycles [1]. Formaldehyde is also a prominent carcinogenic pollutant in the atmosphere [2] and plays an important role in atmospheric chemistry. So, it is highly demanded to improve the spectroscopic data of H_2CO for use in field and laboratory studies. To our knowledge, the spectroscopic data of H_2CO in the near-infrared region is rarely reported in the literatures. The HITRAN 2004 [3] and GEISA 2003 [4] database only provide the data to 3000 cm^{-1} (3−10 μm).

Various spectroscopic methods have been employed in the study of H_2CO. Most of the spectroscopy studies of H_2CO were based on Fourier-transform spectrometer (FTS) [5–9]. The newly developed high-finesse cavity absorption spectroscopy (HFCAS) [10], i.e. cavity ring-down spectroscopy (CRDS) [11], cavity-enhanced absorption spectroscopy (CEAS) [12] and/or integrated cavity output spectroscopy (ICOS) [13], which composed of two or more high-reflectivity mirrors, with typical several kilometers effective optical path length, provided a new high-sensitive method in molecule spectroscopy study, such as CRDS of H_2O and CO_2 [14–17]. The H_2CO absorption spectrum studied by using HFCAS has been reported by Hancock's [18] and Ruth's [19] group. Barry et al. [18] studied the $2\nu_5$ C–H stretching band of H_2CO near 1.76 μm. Staak et al. [19] measured the absorption spectrum of H_2CO from 6548 to 6804 cm^{-1} (1.527−1.470 μm).

*Corresponding author. Fax: +86 551 5591560.
E-mail address: xmgao@aiofm.ac.cn (X. Gao).

0022-4073/$ - see front matter © 2007 Elsevier Ltd. All rights reserved.
doi:10.1016/j.jqsrt.2007.01.057

In this article, we measured the absorption of H_2CO at room temperature by using off-axis integrated absorption spectroscopy (OA-ICOS) with a distributed feedback (DFB) diode laser at 1.573 μm (6351.3−6362.1 cm^{-1}). The formaldehyde molecule has C_{2v} symmetry and six normal modes [19,20]. The spectra region we studied is close to the $\nu_2 + 4\nu_4$ (6346.2 cm^{-1}) and $\nu_3 + 4\nu_6$ (6373.4 cm^{-1}) combination band [21]. The typical sensitivity of our system was about 6×10^{-8} cm^{-1}. More than 140 lines have been recorded within the laser spectral range. The corresponding line parameters (i.e. line positions and line intensities) are presented.

2. Experimental

The experimental set-up is shown in Fig. 1. The light source used was a single-mode InGaAsP DFB diode laser (NTT Electronics Corporation) operating in the near-infrared near 1.573 μm (6357.3 cm^{-1}), without mode hops. The laser power was about 20 mW, and the typical linewidth was ~2 MHz. Frequency tuning of the diode laser could be controlled by scanning either the temperature (~0.42 $cm^{-1}/°C$) or the current (~0.02 cm^{-1}/mA). The temperature and current were controlled by ILX Lightwave LDX-3724B laser diode controller, with short-term (1 h) temperature stability <0.004 °C and long-term (24 h) temperature stability <0.01 °C. The calibration of the laser wavelength was made by a wavemeter (EXFO Burleigh Products Group, WA-1500-NIR) with an accuracy of about ± 0.001 cm^{-1}. Two function generators were used: one was used to dither the cavity length via a piezo transducer (PZT) driver and the other provided a current ramp to tune the laser frequency. The laser's frequency drift is mainly caused by the drift of the ramp from the function generator and the current and temperature unstability, the latter is very small. To characterize the repeatability of each laser current sweep, the absorption line peak positions of different averaging times were compared. The total current drift (ramp and laser) was less than 0.02 mA between 1-sweep and 1000-sweep average (~1-min data aquisition time), the corresponding wavenumber drift less than 0.0005 cm^{-1}.

The laser beam was coupled into a 44-cm OA-ICOS cavity that consisted of two 2.5-cm-diameter spherical mirrors (1.5 m radius of curvature) with a reflectivity of ~99.7%. A Faraday isolator was placed in front of the laser source to minimize the optical feedback from the cavity to the laser. The signal exiting the cavity was focused onto a photodiode and then sent to the computer for further analysis.

The main limitation to the detection sensitivity of the cavity-enhanced spectroscopy method is the cavity-mode noise resulted from the relative intensity fluctuations due to mode injection noise and incomplete averaging of the cavity transmission. Off-axis cavity alignment geometry leads to multiple reflections of the laser radiation in the cavity, which appeared on the mirrors as a series of spots in an elliptical pattern, similar to that in a multipass absorption cell. The effective free-spectral-range (FSR) of the cavity becomes $c/(2md)$,

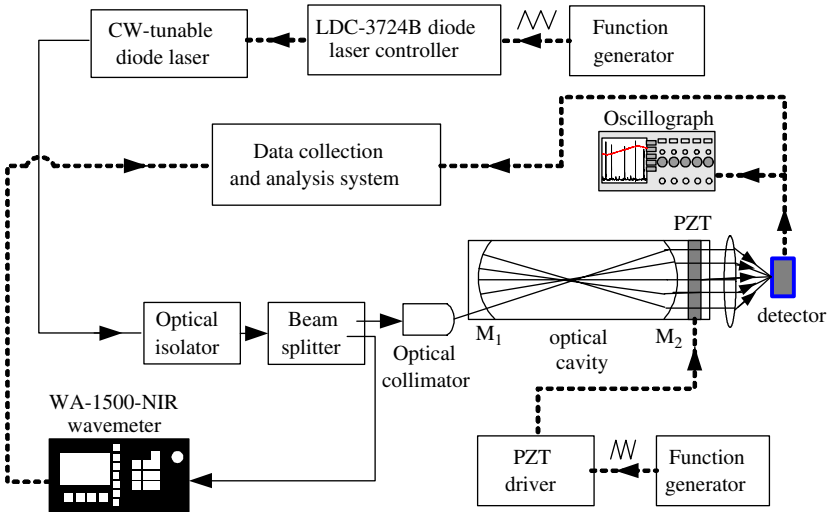

Fig. 1. Experimental set-up of OA-ICOS.

where m is the number of optical round-trip passes and d is the cavity length. An extremely dense-mode spectrum of the cavity can thus be achieved, leads to a more effective average of the cavity-mode transmission. A typical transmitted intensity through the OA-ICOS cavity is shown in the upper panel of Fig. 2(a) (see also Fig. 2 in [22] and Fig. 8 in [23]).

In typical OA-ICOS approach, large peak-to-peak intensity fluctuations were observed, which limit the detection power. To further reduce the fluctuations (referred to as cavity-mode noise effects), we aligned the cavity so that it ceased to be a cavity and had almost no right mode structure characterizing the cavity. The transmission spectra of the cavity and the absorption signals are shown in Fig. 2b. This improved off-axis alignment decreased the peak-to-peak intensity fluctuations of the multimode transmission and improved the detection sensitivity. The signal-noise-ratio was about 22 times improved. The transmission pattern more or less looks like the light intensity pass through a White/Herriott cell in direct absorption spectroscopy, the minimum intensity transmission at a non-zero level and no obvious cavity-mode structure, we referred this transmission pattern as White/Herriott type transmission pattern [24].

A critical design issue for the OA-ICOS is the use of cavity mirrors with a diameter large enough to allow multiple reflections of the laser beam inside the cavity without causing beam overlaps on the mirror surfaces, which will cause the interference effects. Given the diameter of the relative small effective mirrors, only about 8 mm in our experiment, the overlaps of laser beam cannot be avoided. To further reduce the mode effects, a PZT was used to dither the cavity length and partly mechanical vibrations were added to the optical set-up. It was found that the effects of the PZT were small. But in typical transmission pattern, the cavity length dithered by a PZT is useful [23]. So, in our work, we still used a PZT as in typical OA configure. It can partly compensate the insufficiency of off-axis alignment. We intended to remove PZT and mechanical vibration from the cavity in the future.

H_2CO was prepared by pyrolysis of paraformaldehyde (Aldrich, 95% pure) under vacuum [19,25]. The temperature was controlled around 120 °C by an oil bath. The gaseous H_2CO was first passed through a

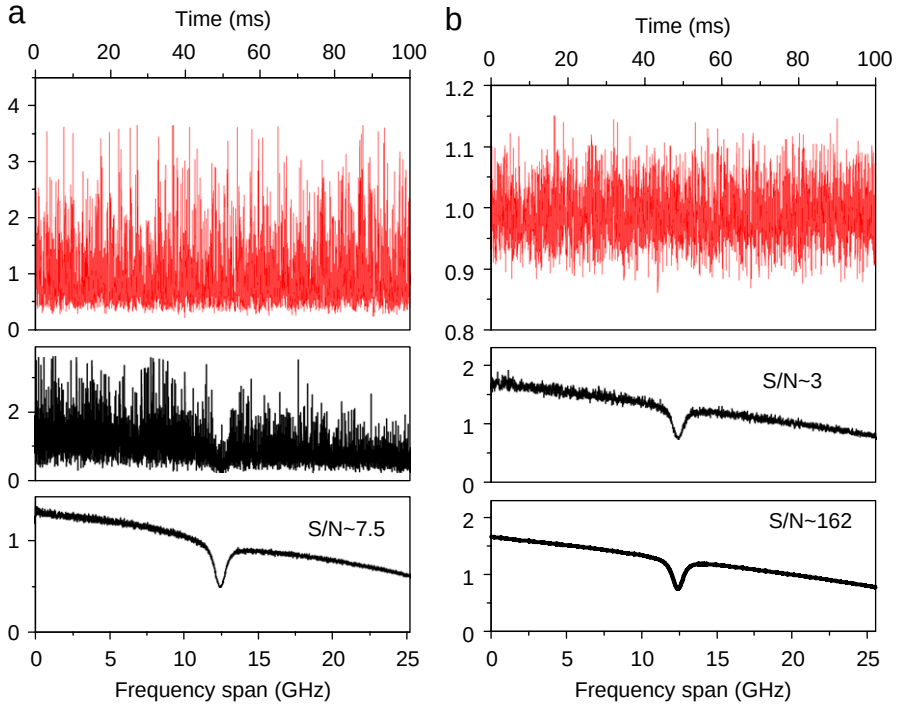

Fig. 2. Transmitted intensity through the ICOS cavity. Upper panels: transmission at a fixed laser frequency. Middle figures: 1-sweep direct intensity transmission spectra of the cavity when scanning the laser (with the presence of a CO_2 absorption feature). Lower curves: results of a 1000-sweep average. (a) Typical OA-ICOS transmission pattern. (b) White/Herriott type transmission pattern.

cooling trap to remove water vapor and polymerization products. The monomeric H_2CO was trapped and stored in liquid nitrogen at 77 K under vacuum.

3. Results and discussion

3.1. Characterizing of the DFB diode laser

In our experiment, frequency tuning of the diode laser was controlled by changing the current injected into the laser diode at each temperature. The laser was scanned over a range of 1 cm^{-1} (referred to as a "spectral segment") using a triangular waveform with a period 20 ms (50 Hz ramp).

To characterize the behaviours of the laser and calibrate the wavelength, the wavelength and current relation was presented at each temperature. The wavenumber was read with a wavemeter. Fig. 3 shows an example of the wavenumber–current relation at laser temperature 23 °C. The current was controlled by a GPIB card and software written in-house, with 1-mA current increment from 40 to 110 mA step-by-step. The time interval of each step was 2 s, which was enough for the stabilization of the wavemeter. Slightly nonlinear tuning properties of the laser was observed. A 3rd order polynomial fit of the data is shown in the figure. The relation at each laser temperature,

$$Wavenumber = a_0 + a_1 \times current + a_2 \times current^2 + a_3 \times current^3, \quad (1)$$

was used for further wavelength calibration. The nonlinear properties were removed from the current tuning and do not affect the lineshape (see Section 3.2 for CO_2 absorption in detail). The small drift of laser frequency each time was re-calibrated by using the absorbers with accurately known line positions, such as NH_3, H_2O, CO_2. After this re-calibration process, an accuracy better than $\pm 0.002\ cm^{-1}$ can be achieved.

3.2. Calibration of the system

ICOS is based on measuring the intensity of light transmitted through a high-finesse optical cavity as a function of wavelength. The light intensity leaking out of the cavity can be written in the form [26]

$$I = I_{in}\frac{(1-R)^2(1-L)}{1-R^2(1-L)^2} = I_0\frac{(1-R)^2\ \exp[-\alpha(v)d]}{1-R^2\ \exp[-2\alpha(v)d]}, \quad (2)$$

where R is the mirror reflectivity (assuming that the reflectivities of the two mirrors are equal), d is the cavity length, I_{in} is the light intensity injected into the cavity, $I_0 = I_{in}(1-R)/(1+R)$ is the light intensity transmitted through the empty cavity (without absorption) and $(1-L) = \exp[-\alpha(v)d]$ when assuming the losses per pass

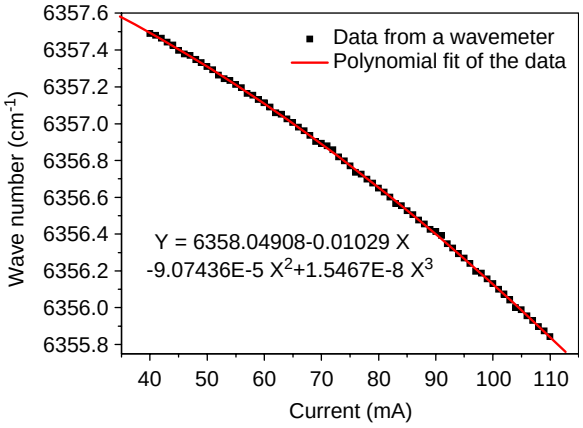

Fig. 3. Characterizing of DFB diode laser. The laser temperature was set to 23 °C. The control of laser injection current and wavelength read from the wavemeter were achieved by a GPIB card and software written in-house, with 1-mA current step. The time interval of each step was 2 s.

resulted solely from linear Lambert–Beers absorption. For small losses per pass and high-reflectivity mirrors, the absorption coefficient can be approximated by [19,26]

$$\alpha \approx \frac{1}{d}\left(\frac{I_0}{I} - 1\right)(1 - R) \tag{3}$$

and the effective optical path length can be determined by $d/(1-R)$.

From Eq. (3), it can be seen that ICOS does not yield absorption cross-sections directly, and the absorption coefficient is proportional to the integrated absorption $((I_0/I)-1)/d$ and the wavelength-dependent mirror reflectivity R. In quantitative analysis application, the mirror reflectivity has to be experimentally determined with either measurements of the cavity ring-down time, or measured absorption spectrum of a calibrated standard species. In the latter case, the mirror reflectivity R can be deduced from the measured integrated absorption $((I_0/I)-1)/d$ with species of known concentration and absorption cross-section, on the basis of Eq. (3). In the present work, the system was calibrated using the integrated cross-sections of CO_2 lines from the HITRAN 2004 [3] database. The calibration process is shown in Fig. 4. Fig. 4(a) shows the raw experimental spectrum of 1.1 torr CO_2. The light intensity transmitted through the empty cavity I_0 was deduced from the polynomial fit result of the baseline. In Fig. 4(b), CO_2 absorption at 6361.25 cm^{-1} at different pressures is presented. The slightly nonlinear tuning properties of the laser was moved out by using Eq. (1). Fig. 4(c) shows the calibration result of the cavity mirror reflectivity via spectrum measurements of CO_2. The y-axis is the integrated absorption $((I_0/I)-1)/d$. The error bars denote the pressure uncertainty.

After calibration, the mirror effective reflectivity 0.99692 ± 0.00007 was achieved at 1.573 μm, the error represents the stand deviation. With a cavity length 44 cm, the effective optical pathlength was about 142.7 m. The error of $(1-R)$ was 2.4%. The pressure uncertainty was about 1%. The system error was estimated to be better than 5%.

3.3. Absorption spectrum

For each spectra segment (~1 cm^{-1}), the spectrum of H_2CO was acquired by the averaging of 3000-sweep with the laser scanning rate of 50 Hz. After considering the electronics speed, the total data aquisition time was

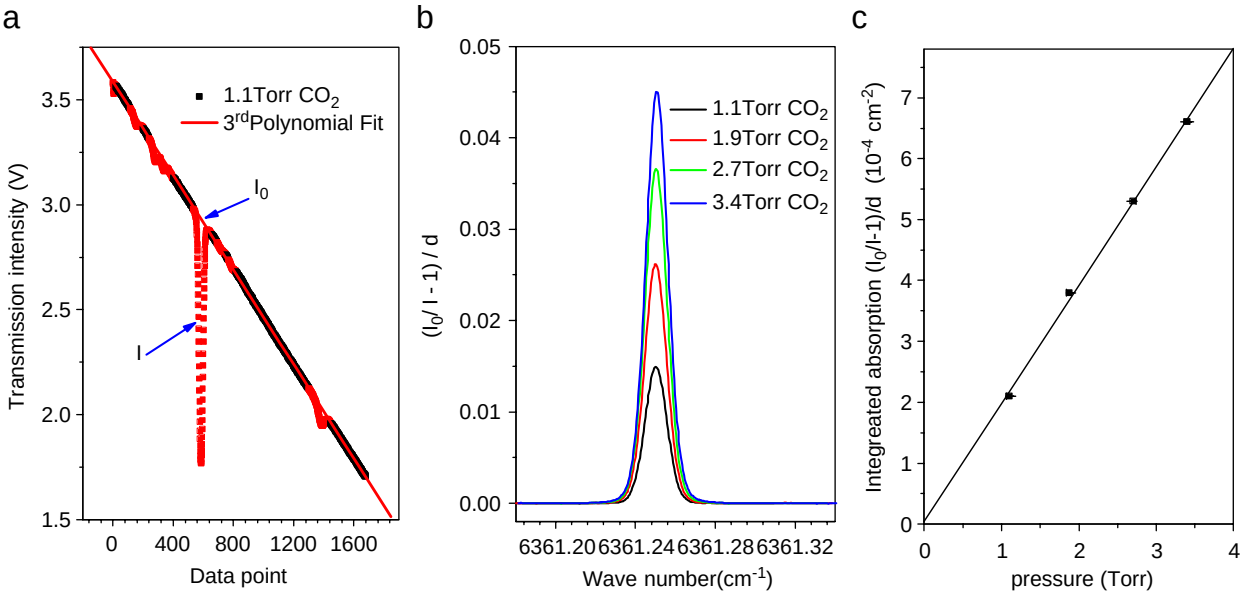

Fig. 4. Calibration process of the cavity mirror reflectivity. (a) Raw experimental spectrum of 1.1 torr CO_2. I_0 was deduced from the polynomial fit result of the baseline. (b) CO_2 absorption at 6361.25 cm^{-1} at different pressures. The slightly nonlinear tuning properties of the laser was moved out. (c) Calibration of the cavity mirror reflectivity via spectrum measurements of CO_2. The y-axis is the integrated absorption $((I_0/I)-1)/d$. The error bars denote the pressure uncertainty.

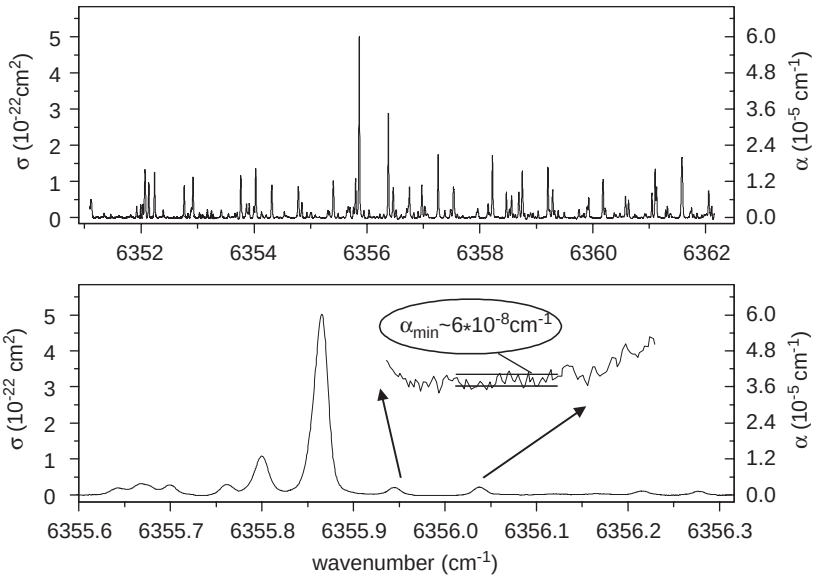

Fig. 5. The absorption spectrum of formaldehyde from 6351.3 to 6362.1 cm^{-1}. The top panel shows the complete spectrum. The lower panel shows the 6355.6−6356.3 cm^{-1} segment. The inset shows the achieved noise level estimated around 6×10^{-8} cm^{-1}.

about 2 min. In each sweep 1680 data points was acquired. The sample interval was about 0.0006 cm^{-1}, which was enough to resolve the Doppler-broadened absorption. The complete absorption spectrum of H_2CO from 6351.3 to 6362.1 cm^{-1} is shown in the top panel of Fig. 5. The lower panel shows the absorption of 6355.6−6356.3 cm^{-1} segment. As illustrated in the inset, a typical noise level of $\alpha_{min} \sim 6 \times 10^{-8}$ cm^{-1} was achieved.

The line positions were determined with two methods. The first method was used to determine the positions of strong lines. In this method, the injection temperature of the laser increased from 12 to 35 °C with 1 °C increment. For each temperature point, the injection current of the laser varies from 30 to 100 mA with 0.03-mA increment. The transmitted intensity of the cavity was recorded together with the corresponding wavelength at each current value without signal averaging. The wavelength was recorded directly from the wavemeter by RS-232 serial interface. By using this method, the accuracy was better than ±0.0015 cm^{-1} and 38 absorption line positions could be known exactly. For weak lines, the line positions were deduced from the wavelength–current relation at each laser temperature. Small error of the weak line positions caused by drift and non-linearity tuning was adjusted by using the strong-line positions measured using the first method. Thus the positions of weak lines could be determined and the accuracy was better than ±0.002 cm^{-1}.

3.4. Line intensity determination

The absorption spectrum was fitted with Voigt line shape by using multispectrum fitting procedure. Fig. 6 shows the result of an unresolved double line H_2CO at 6361.5 cm^{-1}. The top panel shows the absorption spectrum at different pressure. The middle panel is an example of the multispectrum fitting result of 1.3 torr H_2CO spectrum. The scattered symbols represent the experiment data, the solid lines represent the fitted results. The fitted residue is shown in the lower panel. As a result of the fitting, the integrated absorption coefficients for each line were obtained. The integrated absorption coefficients should be proportional to the pressure. The line intensity of each line was obtained from the average result of different spectra.

The line positions, intensities and intensities percentage error of the full range absorption spectrum are listed in Table 1. The average of the overall statistical uncertainty of H_2CO line intensities is about 9%. For the most lines, the uncertainty is around 5%. For some of the weak absorptions, the uncertainty can reach 20%. The percentage error of the line intensities changed between 5% and 20% mainly caused by the errors of I_0

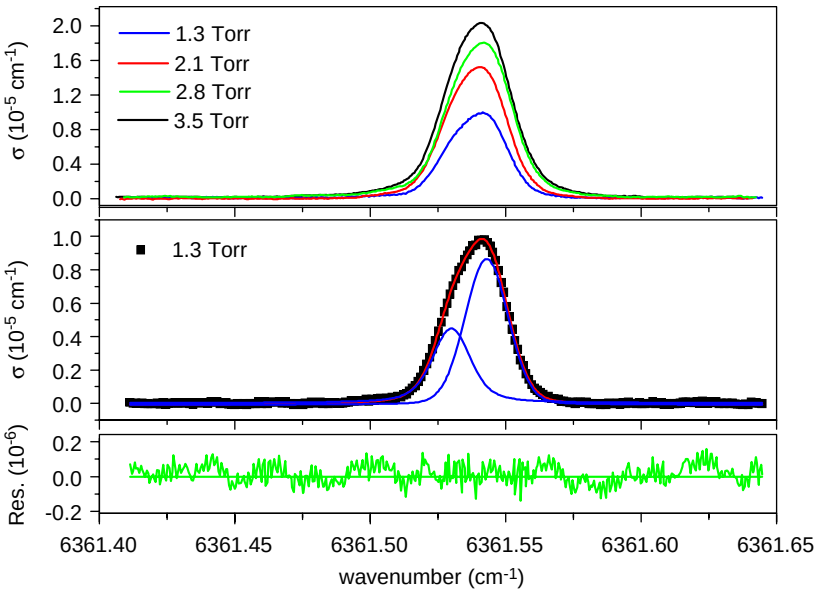

Fig. 6. The unresolved double line at 6361.15 cm^{-1}. The top panel shows the absorption line profile at different pressures. The middle panel: observed (in scattered symbols) and calculated (in solid lines) line profile of 1.3 torr H_2CO, with a multispectrum fitting procedure. The lower panel shows the corresponding fitting residuals.

Table 1
Compilation of the measured line positions and absorption intensities of H_2CO

$\tilde{\nu}$	S	$(\sigma S/S)\%$	$\tilde{\nu}$	S	$(\sigma S/S)\%$	$\tilde{\nu}$	S	$(\sigma S/S)\%$
6351.346	3.49	6.3	6355.489	3.11	11.9	6358.897	4.60	15.7
6351.465	2.23	6.7	6355.652	4.66	2.1	6358.942	2.52	9.5
6351.649	1.65	20.0	6355.676	9.52	4.6	6359.031	4.66	3.2
6351.831	1.23	12.0	6355.703	7.53	4.6	6359.205	32.00	6.3
6351.925	5.88	4.1	6355.763	6.81	9.8	6359.234	4.23	7.1
6351.965	1.05	38.1	6355.800	33.77	2.2	6359.288	17.25	3.4
6351.996	7.54	13.3	6355.856	39.55	15.7	6359.324	3.50	25.7
6352.033	7.04	9.4	6355.865	82.69	4.1	6359.385	5.26	9.9
6352.069	39.61	8.1	6355.944	5.13	5.7	6359.494	3.43	3.4
6352.136	20.01	3.3	6356.038	4.30	3.2	6359.683	0.68	2.2
6352.239	28.12	5.4	6356.215	2.00	3.1	6359.742	6.47	4.3
6352.393	4.21	11.9	6356.277	1.83	11.7	6359.804	2.09	1.2
6352.763	19.97	3.0	6356.379	63.46	3.0	6359.841	2.53	1.7
6352.837	5.60	7.1	6356.464	19.07	3.7	6359.900	8.13	3.3
6352.879	4.60	21.7	6356.515	7.44	7.0	6359.927	12.33	5.2
6352.895	4.28	7.0	6356.608	2.84	24.2	6359.974	1.45	27.6
6352.920	28.20	2.1	6356.716	5.94	7.0	6360.180	23.60	1.4
6353.034	2.40	10.4	6356.739	4.28	3.0	6360.221	6.37	7.8
6353.090	2.95	37.3	6356.760	17.79	5.8	6360.380	3.27	27.5
6353.175	5.78	20.8	6356.829	2.92	3.8	6360.410	2.53	5.9
6353.241	3.64	4.9	6356.907	3.71	8.5	6360.480	2.70	3.3
6353.278	2.37	7.2	6356.973	28.3	3.9	6360.532	0.76	11.8
6353.420	6.73	11.9	6357.028	7.66	11.0	6360.578	19.70	4.9
6353.548	2.55	11.8	6357.058	3.72	19.4	6360.629	12.80	9.2
6353.663	5.00	20.0	6357.077	2.66	22.9	6360.720	1.19	10.9
6353.700	2.86	1.6	6357.260	46.00	2.2	6360.745	4.36	2.4
6353.767	23.11	8.2	6357.277	8.88	11.3	6360.778	1.44	24.3
6353.788	1.91	9.4	6357.380	7.86	10.3	6360.918	3.08	4.5

Table 1 (*continued*)

$\tilde{\nu}$	S	$(\sigma S/S)\%$	$\tilde{\nu}$	S	$(\sigma S/S)\%$	$\tilde{\nu}$	S	$(\sigma S/S)\%$
6353.846	3.17	22.7	6357.477	5.67	10.6	6360.944	1.97	10.2
6353.859	7.56	5.3	6357.490	2.90	5.9	6361.047	14.90	8.7
6353.882	3.43	2.2	6357.529	19.80	4.5	6361.105	26.20	7.6
6353.914	7.76	2.6	6357.543	18.60	3.1	6361.129	17.10	9.4
6354.000	6.96	5.7	6357.600	2.80	2.5	6361.288	4.38	10.7
6354.031	33.01	3.1	6357.699	1.02	2.5	6361.320	7.82	7.7
6354.133	3.70	6.5	6357.897	0.67	26.9	6361.360	2.10	19.0
6354.151	1.85	10.3	6357.941	3.35	3.9	6361.376	3.54	1.9
6354.214	1.80	7.1	6357.964	6.10	10.3	6361.533	18.71	18.2
6354.316	21.84	3.5	6358.150	9.36	2.8	6361.543	38.20	4.2
6354.401	0.65	5.7	6358.172	2.12	26.4	6361.724	4.45	11.9
6354.526	2.85	3.5	6358.223	43.80	5.4	6361.746	5.40	10.2
6354.785	22.73	5.1	6358.481	16.95	5.7	6361.786	1.83	40.4
6354.844	9.68	3.1	6358.530	5.90	16.3	6361.845	3.85	10.4
6354.936	2.66	6.0	6358.567	11.90	13.6	6361.933	1.13	3.7
6355.001	2.13	8.0	6358.596	2.29	13.1	6361.973	1.27	19.7
6355.017	2.54	2.1	6358.630	2.69	11.2	6362.013	1.38	16.7
6355.087	1.78	1.6	6358.691	16.59	2.7	6362.052	15.14	4.0
6355.314	4.36	4.6	6358.752	31.15	5.8	6362.073	1.99	3.0
6355.340	3.13	8.6	6358.791	2.30	4.3	6362.104	6.19	11.3
6355.405	23.30	4.1	6358.855	3.27	0.4			

$\tilde{\nu}$: the spectral line transition frequency (cm^{-1}); S: the spectral line intensity [$10^{-25}\,cm^{-1}/(molecule\,cm^{-2})$]; $(\sigma S/S)\%$: the percent of statistical deviation of line intensities, σS, to the statistical mean value S.

deduced from the baseline and partly caused by the pressure dropped as a result of interaction of the molecules with the walls of tubing and of the stainless-steel cell because of its relatively large dipole moment (2.3 D).

4. Conclusions

We have recorded the spectrum of H_2CO at 1.573 μm (6351.3−6362.1 cm^{-1}) at room temperature by using OA-ICOS technique. Line positions and intensities are presented. In ICOS, the laser frequency is scanned rapidly over a spectral region, and the light intensity leaked out of the cavity is detected. This results in a flat cavity transmission with frequency on which to observe the molecule absorption features, which makes ICOS looks more or less like traditional direct absorption spectroscopy. In ICOS, the mirror reflectivity R or effective pathlength $l_{\text{eff.}}$ is only an interim quantity. The error of line intensity mainly caused by the accuracy of the cross-sections according to HITRAN used for the mirror reflectivity calibration. ICOS provide a highly precise technique for spectrum studies.

References

[1] Pope FD, Smith CA, Davis PR, Shallcross DE, Ashfold MNR, Orr-Ewing AJ. Photochemistry of formaldehyde under tropospheric conditions. Faraday Discuss 2005;130:59–72.
[2] Dahnke H, von Basum G, Kleinermanns K, Hering P, Murtz M. Rapid formaldehyde monitoring in ambient air by means of mid-infrared cavity leak-out spectroscopy. Appl Phys B 2002;75:311–6.
[3] Rothman LS, Jacquemart D, Barbe A, Chris Benner D, Birk M, Brown LR, et al. The HITRAN 2004 molecular spectroscopic database. JQSRT 2005;96:139–204.
[4] Jacquinet-Husson N, Scott NA, Chedina A, Garceran K, Armante R, Chursin AA, et al. The 2003 edition of the GEISA/IASI spectroscopic database. JQSRT 2005;95:429–67.
[5] Reuter DC, Nadler S, Daunt SJ, Johns JWC. Frequency and intensity analysis of the v_3, v_4, and v_6 bands of formaldehyde. J Chem Phys 1989;91:646–54.
[6] Ito F, Nakanaga T, Takeo H. FTIR spectra of the $2v_4$, $v_4 + v_6$ and $2v_6$ bands of formaldehyde. Spectochim Acta A 1994;50:1397–412.

[7] Perrin A, Keller F, Flaud J-M. New analysis of the ν_2, ν_3, ν_4, and ν_6 bands of formaldehyde $H_2^{12}C^{16}O$ line positions and intensities in the 5−10 μm spectral region. J Mol Spectrosc 2003;221:192–8.
[8] Lohilahti J, Ulenikov ON, Bekhtereva ES, Horneman V-M, Alanko S. The fundamental bands ν_3, ν_4, and ν_6 of $D_2^{13}CO$. J Mol Spectrosc 2005;231:108–16.
[9] Co DT, Hanisco TF, Anderson JG, Keutsch FN. Rotationally resolved absorption cross sections of formaldehyde in the 28100−28500 cm^{-1} (351−356 nm) spectral region: implications for in situ LIF measurements. J Phys Chem A 2005;109:10675–82.
[10] Brown SS. Absorption spectroscopy in high-finesse cavities for atmospheric studies. Chem Rev 2003;103:5219–38.
[11] O'Keefe A, Deacon DA. Cavity ring-down optical spectrometer for absorption measurements using pulsed laser sources. Rev Sci Instrum 1988;59:2544–51.
[12] Engeln R, Berden G, Peeters R, Meijer G. Cavity enhanced absorption and cavity enhanced magnetic rotation spectroscopy. Rev Sci Instrum 1998;69:3763–9.
[13] O'Keefe A, Scherer JJ, Paul JB. CW integrated cavity output spectroscopy. Chem Phys Lett 1999;307:343–9.
[14] Ding Y, Macko P, Romanini D, Perevalov VI, Tashkun SA, Teffo JL, et al. High sensitivity CW-cavity ringdown and Fourier transform absorption spectroscopies of $^{13}CO_2$. J Mol Spectrosc 2004;226:146–60.
[15] Macko P, Romanini D, Mikhailenko SN, Naumenko OV, Kassi S, Jenouvrier A, et al. High sensitivity CW-cavity ring down spectroscopy of water in the region of the 1.5 μm atmospheric window. J Mol Spectrosc 2004;227:90–108.
[16] Majcherova Z, Macko P, Romanini D, Perevalov VI, Tashkun SA, Teffo JL, et al. High-sensitivity CW-cavity ringdown spectroscopy of $^{13}CO_2$ near 1.5 μm. J Mol Spectrosc 2005;230:1–21.
[17] Naumenko O, Sneep M, Tanaka M, Shirin SV, Ubachs W, Tennyson J. Cavity ring-down spectroscopy of $H_2^{17}O$ in the range 16570−17125 cm^{-1}. J Mol Spectrosc 2006;237:63–9.
[18] Barry H, Corner L, Hancock G, Peverall R, Ritchie GAD. Cross sections in the 2ν5 band of formaldehyde studied by cavity enhanced absorption spectroscopy near 1.76 μm. Phys Chem Chem Phys 2002;4:445–50.
[19] Staak M, Gash EW, Venables DS, Ruth AA. The rotationally-resolved absorption spectrum of formaldehyde from 6547 to 6804 cm^{-1}. J Mol Spectrosc 2005;229:115–21.
[20] Poulin NM, Bramley MJ, Carrington Jr R, Kjaergaard HG, Henry BR. Calculation of vibrational ($J = 0$) excitation energies and band intensities of formaldehyde using the recursive residue generation method. J Chem Phys 2002;104:7807–20.
[21] Bouwens RJ, Hammerschmidt JA, Grzeskowiak MM, Stegink TA, Yorba PM, Polik WF. Pure vibrational spectroscopy of S_0 formaldehyde by dispersed fluorescence. J Chem Phys 1996;104:460–79.
[22] Malara P, Maddaloni P, Gagliardi G, DeNatale P. Combining a difference-frequency source with an off-axis high-finesse cavity for trace-gas monitoring around 3 μm. Opt Express 2006;14:1304–13.
[23] Bakhirkin YA, Kosterev AA, Roller C, Curl RF, Tittel FK. Mid-infrared quantum cascade laser based off-axis integrated cavity output spectroscopy for biogenic nitric oxide detection. Appl Optics 2004;43:2257–66.
[24] Zhao W, Gao X, Chen W, Zhang W, Huang T, Wu T, et al. Wavelength modulated off-axis integrated cavity output spectroscopy in the near infrared. Appl Phys B 2007;86:353–9.
[25] Burkart M, Schramm B. Foreign gas broadening of an IR absorption line of formaldehyde. J Mol Spectrosc 2003;217:153–6.
[26] Fiedler SE, Hese A, Ruth AA. Incoherent broad-band cavity-enhanced absorption spectroscopy. Chem Phys Lett 2003;371:284–94.